Biochimica et Biophysica Acta 1807 (2011) 68–79

Contents lists available at ScienceDirect

Biochimica et Biophysica Acta

journal homepage: www.elsevier.com/locate/bbabio

Biochemical and biophysical characterization of succinate: Quinone reductase from *Thermus thermophilus*

Olga Kolaj-Robin [a,1], Sarah R. O'Kane [a,1], Wolfgang Nitschke [b], Christophe Léger [b], Frauke Baymann [b], Tewfik Soulimane [a,*]

[a] Chemical and Environmental Sciences Department and Materials & Surface Science Institute, University of Limerick, Limerick, Ireland
[b] Laboratoire de Bioénergétique et Ingénierie des Protéines, IFR88, CNRS, 31, chemin Joseph Aiguier, 13402 Marseille cedex 20, France

ARTICLE INFO

Article history:
Received 15 June 2010
Received in revised form 5 October 2010
Accepted 6 October 2010
Available online 14 October 2010

Keywords:
Complex II
Succinate:quinone oxidoreductase
Succinate dehydrogenase
Cooperativity
Thermus thermophilus

ABSTRACT

Enzymes serving as respiratory complex II belong to the succinate:quinone oxidoreductases superfamily that comprises succinate:quinone reductases (SQRs) and quinol:fumarate reductases. The SQR from the extreme thermophile *Thermus thermophilus* has been isolated, identified and purified to homogeneity. It consists of four polypeptides with apparent molecular masses of 64, 27, 14 and 15 kDa, corresponding to SdhA (flavoprotein), SdhB (iron–sulfur protein), SdhC and SdhD (membrane anchor proteins), respectively. The existence of [2Fe–2S], [4Fe–4S] and [3Fe–4S] iron–sulfur clusters within the purified protein was confirmed by electron paramagnetic resonance spectroscopy which also revealed a previously unnoticed influence of the substrate on the signal corresponding to the [2Fe–2S] cluster. The enzyme contains two heme *b* cofactors of reduction midpoint potentials of −20 mV and −160 mV for b_H and b_L, respectively. Circular dichroism and blue-native polyacrylamide gel electrophoresis revealed that the enzyme forms a trimer with a predominantly helical fold. The optimum temperature for succinate dehydrogenase activity is 70 °C, which is in agreement with the optimum growth temperature of *T. thermophilus*. Inhibition studies confirmed sensitivity of the enzyme to the classical inhibitors of the active site, as there are sodium malonate, sodium diethyl oxaloacetate and 3-nitropropionic acid. Activity measurements in the presence of the semiquinone analog, nonyl-4-hydroxyquinoline-N-oxide (NQNO) showed that the membrane part of the enzyme is functionally connected to the active site. Steady-state kinetic measurements showed that the enzyme displays standard Michaelis–Menten kinetics at a low temperature (30 °C) with a K_M for succinate of 0.21 mM but exhibits deviation from it at a higher temperature (70 °C). This is the first example of complex II with such a kinetic behavior suggesting positive cooperativity with *k'* of 0.39 mM and Hill coefficient of 2.105. While the crystal structures of several SQORs are already available, no crystal structure of type A SQOR has been elucidated to date. Here we present for the first time a detailed biophysical and biochemical study of type A SQOR—a significant step towards understanding its structure–function relationship.

1. Introduction

Enzymes serving as respiratory complex II belong to the succinate: quinone oxidoreductases (SQOR) superfamily (EC 1.3.5.1). Members of this group can be classified depending on the direction of the reaction they catalyze *in vivo*. Succinate:quinone reductases (SQRs) mediate oxidation of succinate to fumarate coupled with reduction of quinone to quinol, whereas the reverse reaction of quinol oxidation coupled to fumarate reduction is catalyzed by quinol:fumarate reductases (QFRs) [1]. Succinate:quinone reductases are involved in aerobic metabolism and, as well as being a part of the respiratory chain, they constitute the only membrane-bound enzyme of the tricarboxylic acid cycle [2]. In contrast, QFRs participate in anaerobic respiration with fumarate as the terminal electron acceptor [3]. SQR and QFR are homologous proteins evolved from a common evolutionary ancestor, and has been shown to catalyze both reactions *in vivo* and *in vitro*; they are functional replacements of each other when the appropriate conditions are met [4,5]. SQORs typically consist of three to four subunits: the hydrophilic subunits A and B containing the flavin cofactor and [2Fe–2S], [4Fe–4S], and [3Fe–4S] iron–sulfur clusters, respectively, and one large or two small membrane-bound subunits (C or C and D). SdhA and SdhB are highly conserved among members of all domains of life while the sequence similarities between the membrane domains of complex II are significantly lower. The dicarboxylate oxidation/reduction and quinone reduction/oxidation sites are located in the subunit A and in the membrane

* Corresponding author. Tel.: +353 61234133; fax: +353 61202568.
E-mail address: tewfik.soulimane@ul.ie (T. Soulimane).
[1] Both authors contributed equally to this work.

0005-2728/$ – see front matter © 2010 Elsevier B.V. All rights reserved.
doi:10.1016/j.bbabio.2010.10.009

anchor subunit(s), respectively. Several classification systems have been proposed for complex II [1,6–9], with the one based on the number of membrane-bound domains and differences in heme *b* composition being the most commonly accepted. It distinguishes five types of SQORs: A, B, C, D and E. Enzymes with only one membrane subunit fall into type B as opposed to the all other types containing two hydrophobic domains. The heme content varies between zero (type D and E), one (type C) and two (types A and B). Type E comprises the so-called non-classical SQORs containing two hydrophobic subunits with properties significantly different from that of types A-D [10,11]. Interestingly, recent findings showed that the "non-classical" (type E) SQOR from *Wolinella succinogenes* is a QFR with no SQR activity [12]. The first three-dimensional structure of membrane-bound complex II, a D-Type QFR from *Escherichia coli* [13], was published in June 1999 and shortly after, the structure of a B-type QFR from *W. succinogenes* followed [14]. A few years later, the structure of a C-type SQR from *E. coli* became available [15]. In addition to these prokaryotic enzymes, two mitochondrial complexes II have also been solved recently: SQRs from avian heart [16] and from porcine heart [17], both of them representing type C SQORs. Yet, a crystal structure of a type A SQOR is still missing. Moreover, although recent evidence suggests the structural function of heme *b* in the molecule and its role in maintaining a high rate of catalysis [18,19], the detailed function of heme *b* remains controversial despite the availability of several 3D structures of complex II. Even though steps to elucidate the crystal structure of the first thermophilic QFR from the photosynthetic bacterium *Chloroflexus aurantiacus* have been made [20], we describe for the first time the biochemical and biophysical properties of the SQR from an extremely thermophilic organism, *Thermus thermophilus.* While the respiratory chain complexes from this organism are widely studied, description of complex II has not been reported. To date, only the crystal structures of the respiratory complex I (NADH dehydrogenase) [21] and one of two *T. thermophilus* complexes IV (ba_3 cytochrome *c* oxidase) [22] have been determined. In addition, the work described herein provides for the first time an extensive characterization of the type A SQOR and represents a significant step towards the determination of the first crystal structure of type A complex II comprising two membrane anchor subunits and two heme cofactors. This will improve our understanding of the role of heme *b* in complex II and the functional mechanism of this important family of proteins.

2. Materials and methods

2.1. Fermentation of T. thermophilus HB8

Fermentation of *T. thermophilus* HB8 has been performed at the Helmholtz Centre for Infection Research, Braunschweig, Germany as described previously [23]. The low oxygen tension condition is not required for efficient expression of complex II and was used to simultaneously obtain a larger amount of another respiratory chain complex, ba_3 cytochrome *c* oxidase.

2.2. Isolation of membrane proteins

One hundred grams of *T. thermophilus* cells were resuspended with 500 mL of 0.25 M Tris–HCl (pH 7.6) buffer containing 0.2 M KCl and homogenized. Subsequently, lysozyme was added to a final concentration of 0.6 μM and the suspension was stirred for 3 h at 4 °C. After sample centrifugation at 53,936*g* for 45 min at 4 °C, the supernatant containing *T. thermophilus* soluble proteins was discarded and the pellet was resuspended with 500 mL of 0.1 M Tris–HCl (pH 7.6), homogenized and centrifuged at 53,936*g* for 30 min at 4 °C. This washing step is repeated three times to further remove the periplasmic and cytoplasmic proteins. The pellet resulting after the washings was resuspended in 500 mL of 0.1 M Tris–HCl (pH 7.6) and incubated for 3 h at 4 °C in the presence of 5% Triton X-100 (Sigma Aldrich) in order to solubilize the membrane proteins. Non-solubilized proteins were removed by centrifugation at 53,936*g* for 1 h at 4 °C.

2.3. Purification of complex II

The solubilized membrane proteins were diluted with cold MiliQ water up to 5 L to decrease the detergent concentration to 0.1% Triton and the conductivity to <2 mS/cm. The proteins were then chromatographed on an anion exchange chromatography at 4 °C using a 30×10 cm column packed with DEAE-Biogel agarose (Biorad) equilibrated with 0.01 M Tris–HCl (pH 7.6), 0.1% Triton X-100. The column with firmly-bound respiratory chain complexes was washed with 2 L of 0.01 M Tris–HCl (pH 7.6), 0.1% Triton X-100. Elution with 4 L (2×2 L) of linear gradient from 0 to 0.25 M NaCl resulted in three distinct peaks containing, among others, the respiratory chain complexes identifiable based on their corresponding reduced-minus-oxidized spectra in the region between 400 and 650 nm [23]. The complex II-containing fractions were pooled, dialysed against 0.01 M Tris–HCl (pH 7.6), 0.1% Triton X-100 buffer and subjected to a series of further chromatographic steps performed using the Äkta Prime or Äkta Explorer systems (GE Healthcare). Firstly, the dialysed sample was loaded on a XK 26/20 column, packed with 30 mL of Fractogel EMD TMAE (Merck) previously equilibrated with 0.01 M Tris–HCl (pH 7.6), 0.1% Triton X-100. After sample binding to the resin, a detergent exchange step was performed by washing the column extensively with 0.01 M Tris–HCl (pH 7.6), 0.05% dodecyl-ß-D-maltoside (DDM) (Anatrace, USA) until Triton X-100 has been removed from the sample, as determined from the 280 nm absorbance contribution of Triton X-100. Elution was performed with a linear gradient of 0 to 0.5 M NaCl, for 1 h at a flow rate of 4 mL/min. Complex II-rich fractions were pooled and concentrated to 2 mL using a centrifugal filter (Centricons YM100, Millipore) and applied on Highload XK 16/60 Superdex 200 gel filtration column (GE-Healthcare) previously equilibrated with 0.05 M Tris–HCl (pH 7.6), 0.05% DDM. The complex II sample resulting from gel filtration was diluted in 1:100 ratio with 0.01 M sodium phosphate (pH 6.8), 0.05% DDM buffer and applied on XK 16/20 column, filled with 20 mL of hydroxylapatite "high resolution" resin (Fluka, BioChemika), pre-equilibrated with the same buffer. The complex II was eluted with a linear gradient from 0.01 M to 0.04 M of sodium phosphate (pH 6.8), 0.05% DDM within 0.5 h at a flow rate 2 mL/min. Subsequently, complex II sample was diluted with 0.01 M Tris–HCl (pH 7.6), 0.05% DDM buffer to reduce the sample conductivity to below 2 mS/cm and the ion exchange with Fractogel EMD TMAE (Merck) and gel filtration chromatography (Superdex 200, GE Healthcare) steps were repeated as described above, resulting in purified complex II. The protein was concentrated to 10–15 mg/mL (Centricons YM100, Millipore), aliquoted and snap frozen at −80 °C.

2.4. Determination of protein concentration

Reduced-minus-oxidized spectra in the range 650 nm to 400 nm were recorded using a Perkin Elmer Lambda 35 UV/Vis spectrophotometer. Heme *b* concentration was calculated from the reduced-minus-oxidized spectrum at 558 nm using a molar absorption coefficient of 17,000 M^{-1} cm^{-1} calculated based on the pyridine hemochrome spectra as described elsewhere [24]. The reduced spectra were obtained by adding a few grains of solid sodium dithionite to the air-oxidised sample.

2.5. Peptide separation by HPLC

The subunits of the *T.thermophilus* complex II were purified on a reversed phase Synchropak C_4 column (250×4.6 mm) using a

Hewlett-Packard 1050 HPLC system with a multiple wavelength detector and the following solvents: (1) 8% formic acid, (2) 92% formic acid, (3) n-propanol, and (4) acetonitril. Gradients were formed with a microprocessor-controlled quaternary pump (HP) by low-pressure mixing of the four solvents in 60 min: (1) 14% to 0%, (2) 70%= constant, (3) 6% to 30%, and (4) 10% to 0% (by vol.).

2.6. Amino acid sequencing

Automated Edman degradation [25] was performed using Knauer 910 gas/liquid-phase protein sequencer on polybrene coated PVDF membranes with autoconversion and on-line HPLC identification of the phenylthiohydantoin amino acids. 500 pmoles of single subunits isolated by HPLC was directly used for sequencing. Integral complex II has also been applied for sequencing demonstrating the stoichiometrical presence of all subunits.

2.7. Blue Native PAGE

The Blue Native PAGE (BN-PAGE) was performed in 8% acrylamide gels as described elswhere [26]. Apoferritin from horse spleen (Sigma Aldrich #A3660) and β-amylase from sweet potato (Sigma Aldrich #A8781) were used as markers to indicate the molecular weights.

2.8. CD spectroscopy

CD analysis was performed using a Chirascan circular dichroism spectrometer (Applied Photophysics) and quartz suprasil (QS) cuvettes of 0.1 mm path length (Hellma GmbH). Baseline spectra in each buffer and spectra for protein samples were collected in triplicate at wavelengths from 180 to 280 nm with 4 s time points and 1 nm bandwidth. Chirascan Pro-Data software was used for data acquisition. Baselines and protein spectra were separately averaged, and the averaged baselines were subtracted from the relevant averaged protein spectra and smoothed. Complex II was analyzed at a concentration of 1 mg/mL in 50 mM Tris–HCl (pH 7.6), 0.02% DDM. Secondary structure elements were calculated with the CDNN software (CD Spectra Deconvolution v.2.1; [27]).

2.9. Redox titration

Redox titrations of the purified complex II were performed electrochemically in an optical thin layer electrochemical cell at room temperature. Purified enzyme samples were analysed in 50 mM MOPS (pH 7) with 0.01% DDM and 50 mM KCl in the presence of the phenazine ethosulfate, duroquinone, 2,5-dihydroxy-p-benzoquinone and dihydroxy-1,4-naphthoquinone as redox mediators at 10 μM final concentration each. In addition a redox titrtaion in the presence of 500 mM nonyl-4-hydroxyquinoline-N-oxide (NQNO) was carried out. All titrations were performed in oxidative and reductive directions in steps of 50 mV. An equilibration time of 5 min proved to be sufficient for the redox reactions to reach equilibrium. Optical spectra were recorded between 400 nm and 600 nm on a Cary 5E spectrophotometer. The titrations were performed as a single experiment and were evaluated on the Soret band at 427 nm minus 411 nm by fitting the amplitude of the signal to a sum of two $n=1$ Nernst equations in order to determine the redox midpoint potential of the *b*-hemes.

2.10. EPR spectroscopy

EPR spectra were recorded on a Bruker ElexSys X-band spectrometer fitted with an Oxford Instrument He-cryostat and temperature control system. 2 mM EDTA was added to the samples of the purified enzyme. Buffers used were either 50 mM MOPS (pH 7) or 200 mM AMPSO (pH 9). Samples were reduced by the addition of 5 mM ascorbate, 120 mM succinate (from a 1 M stock solution in water) or dithionite (from a 200 mM stock solution in 500 mM CAPS pH 10). Additions of reducing agents were performed at room temperature followed by vortexing and freezing of the sample in liquid nitrogen within 5 min after addition. Protein concentration was 20 μM (for experiments with ascorbate) or 70 μM (for experiments with succinate and dithionite).

Redox titrations on membrane fragments were performed as described by Dutton [28] in the presence of mediators: neutral red, safranine T, anthraquinone-2-sulfonate, anthraquinone-2,6-disulfonate, indigocarmine, 1,4-dimethyl-naphthoquinone, phenazine methyl sulfate at a concentration of 100 M each. Reductive and oxidative titrations were carried out using sodium dithionite and ferricyanide, respectively.

2.11. Cyclic voltammetry

Protein film voltammetry experiments [29] were performed in a glovebox (JACOMEX) filled with N_2 (residual $O_2<1$ ppm), using the electrochemical setup and equipment described previously [30]. The two-compartment electrochemical cell was thermostated at the desired temperature value using a water circulation system. The rotating pyrolytic graphite edge working electrode (PGE) (area $A\approx 3\ mm^2$) was used in conjunction with an electrode rotator, a platinum wire was used as a counter electrode, and a saturated calomel electrode (SCE), located in a side arm containing 0.1 M NaCl and maintained at room temperature, was used as a reference. All potentials are quoted versus the standard hydrogen electrode (SHE), ($E^{SHE}=E^{SCE}+240$ mV). The electrochemical cell contained a buffer consisting of 50 mM Tris and 0.1 M NaCl titrated to pH 7 or 8.5. The substrates were added from stock solutions of 0.4 M fumarate at pH 7 or 1 M succinate at pH 8.5.

The protein films were prepared by painting the freshly-polished electrode with about 0.5 μL of a stock enzyme solution (35 μM of enzyme in the Tris/NaCl buffer at pH 7) followed by drying. The enzyme-coated electrode was inserted in the electrochemical cell containing the buffer mixture at pH 8.5, 50 °C, in the presence of 1 mM succinate, and the enzyme films were activated by cycling the electrode potential between −360 mV and +240 mV *vs* SHE at 20 mV/s, while the electrode was rotated at 3000 rpm, for ~15 min, during which the succinate oxidation current increased as a consequence of enzyme activation and then stabilized. The electrode was then transferred to a fresh buffer.

2.12. Activity measurements

Succinate-2,6-dichlorophenolindophenol (DCPIP) oxidoreductase activity was measured spectroscopically by following the reduction in the absorbance changes of DCPIP at 600 nm using Cary 300 Bio UV-VIS spectrophotometer accessorised with Varian Cary dual cell Pelteir unit. The millimolar extinction coefficient used for DCPIP was 20.7 $mM^{-1}\ cm^{-1}$ [31]. The reaction mixture contained 50 mM Tris–HCl buffer (pH 8.5), 0.02% DDM, 400 μM phenazine methosulfate (PMS), 0.01–5 mM sodium succinate and 100 μM DCPIP. The reaction was initiated by addition of DCPIP into the mixture of PMS and the enzyme previously activated by incubation with succinate at 30 °C for 30 min or at 70 °C for 5 min. Furthermore, enzyme activity was assayed at 30 °C with DCPIP only and in the presence of DCPIP and menadione, duroquinone (DQ), 1,4-naphthoquinone (1,4-NQ) or p-benzoquinone (p-BQ) at 1 mM final concentration.

Inhibition of succinate oxidation activity by 0–0.4 mM sodium malonate, 0–0.5 mM sodium diethyl oxaloacetate, 0–5 mM 3-nitropropionic acid (3-NP) and 0–0.03 mM nonyl-4-hydroxyquinoline-N-oxide (NQNO) was tested with PMS/DCPIP or 1,4-NQ/DCPIP as electron acceptor as indicated in Results section.

All characterisations were performed with a complex II concentration of 40 nM at 30 °C and 10 nM at 70 °C. Data were processed

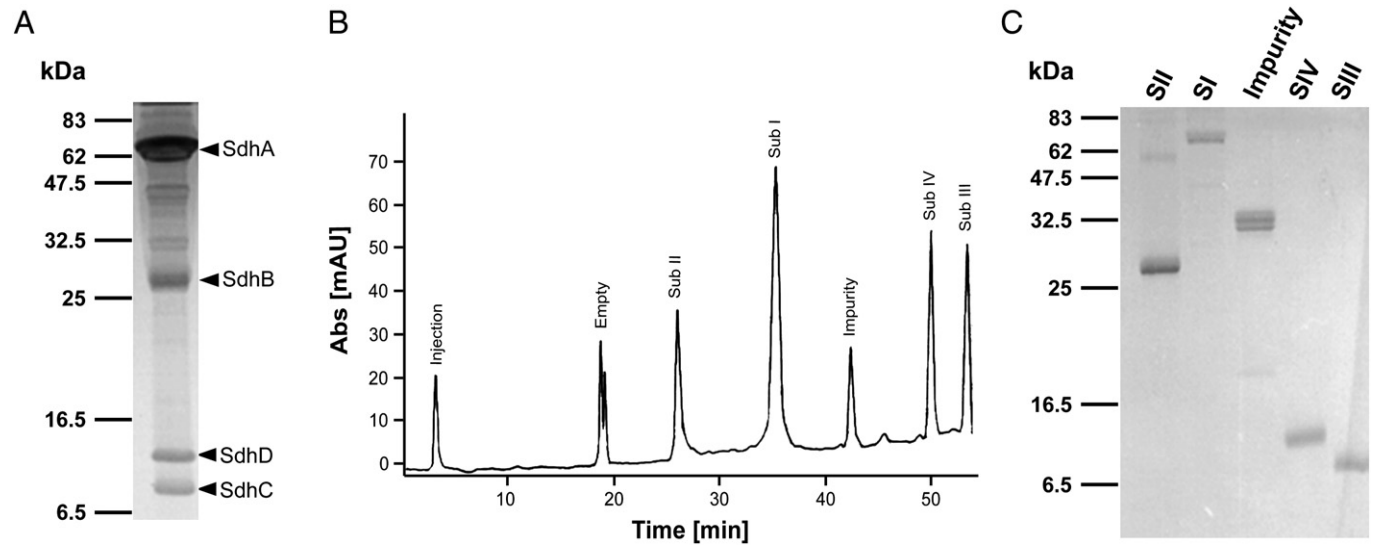

Fig. 1. Identification of subunits of complex II from *T. thermophilus*. A—SDS-PAGE analysis of isolated complex; B—HPLC separation of the subunits; C—SDS-PAGE analysis of HPLC-separated fractions.

with GraphPad Prism 5 using the $V_0 = V_{max} \times [S]^h/(k' + [S]^h)$ equation for cooperative sigmoidal kinetics.

2.13. Protein crystallization

Crystallization of the complex II was performed using the sitting-drop vapor-diffusion method. The protein solution of concentration 15 mg/mL was equilibrated in CrysChem plates (Supper Charles Company) against 500 μL reservoir solution at 20 °C. Each droplet was prepared by mixing equal volumes (1 μL) of protein and reservoir solutions. Crystal hits were obtained in condition no. 37 of Crystal Screen Lite (0.1 M sodium acetate trihydrate pH 4.6, 4% (w/v) polyethylene glycol 4000) and condition no. 11 of MembFac (0.1 M magnesium chloride hexahydrate, 0.1 M sodium acetate trihydrate pH 4.6, 12% (w/v) polyethylene glycol 6000) screens (Hampton Research) and the process was further optimized using fine intervals of precipitant concentration and pH as well as various combinations of salt additives. The crystals grown for one week reached dimensions of up to 160 × 50 × 40 μm.

3. Results and discussion

3.1. Isolation and purification of complex II from T. thermophilus

For characterization and subsequent crystallization of complex II from *T. thermophilus*, a method of isolation and generation of highly-pure enzyme has been developed. Its initial stages have been described previously for isolation of the ba_3 cytochrome *c* oxidase [23] and involve solubilization of *T. thermophilus* membrane proteins and DEAE Biogel (Biorad)-based anion exchange chromatography which had proven useful in primary separation of *T. thermophilus* respiratory chain proteins. Heme-rich respiratory chain complexes can be distinguished based on their corresponding reduced-minus-oxidized spectra in the region between 400 and 650 nm. Therefore, the three peaks shown on the chromatogram from the initial ion exchange chromatography [32] can be easily identified as fractions containing mainly ba_3-, caa_3-type cytochrome *c* oxidase and a mixture of various cytochromes together with complex II, respectively [23]. The main difficulty in the further purification of complex II lies in removal of *bc* complex (complex III) which continuously dissociates into the constituent cytochromes b_{562} and $c_{554/548}$, as well as the residual caa_3 cytochrome *c* oxidase and another cytochrome, b_{560}. While cytochrome b_{562} is removed during the second chromatography as it does not bind to the Fractogel EMD TMAE material (Merck), the majority of caa_3 present is separated from complex II during this purification step. The cytochrome $c_{554/548}$, the so-called split α-cytochrome, is easily removed during the first gel filtration step due to the low molecular weight of the heme binding domain (11 kDa). Subsequent chromatography with hydroxylapatite resin (Fluka Biochemica) not only leads to the removal of the persistent heme-less proteins but also seemed to promote complete disassembly of *bc* complex into the cytochromes b_{562} and $c_{554/548}$ and their efficient removal; residual caa_3-oxidases is also removed in this step. The repeated ion exchange chromatography on Fractogel EMD TMAE was employed to ensure complete removal of any remaining heme-rich and heme-less proteins, which resulted in a single peak after the final gel filtration chromatography run. The described purification procedure yielded ~8 mg of pure enzyme from 100 g of *T. thermophilus* biomass (Fig. 1A). The content of heme *b* in the purified sample was 16.38 nmol/mg of protein (Table 1), which is very close to the theoretical value of 16.6 nmol/mg of protein considering the molecular weight of the complex as 119.78 kDa and the existence of two hemes per protein monomer.

Table 1
Purification of succinate:quinone oxidoreductase from *Thermus thermophilus*.

Purification step	Total protein (mg)	Heme content (nmol)	Heme/protein ratio (mg/nmol)	Yield (%)
DEAE-Biogel	264.0	290	1.06	100
TMAE	49.2	210	4.27	75
Gel filtration	29.2	196	6.71	70
Hydroxyapatite	15.2	188	12.37	67
TMAE	10.8	157	14.53	56
Gel filtration	8.0	131	16.38	47

Table 2
Results of the N-terminal sequencing of separated subunits of *Thermus thermophilus* succinate:quinone oxidoreductase.

Subunit	N-terminal sequencing results
II (Sdh B)	MQVTLKVLRFDPAKDKKPRWETYQVEAEPWDRVLDLLH
I (Sdh A)	MAHRHEVIVVGAGGAGLTAALYAAKEGADVAVVSK
IV (Sdh D)	MAIKSKRYQEARLEASTNLELYWWVFMR
III (Sdh C)	MYRGSEGQWAFYLHRIS

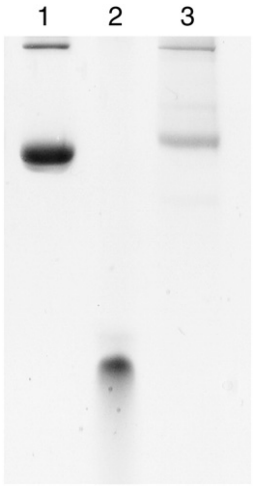

Fig. 2. Blue Native PAGE analysis of complex II. Lanes: 1—apoferritin monomer (443 kDa) and dimer (886 kDa), 2—β-amylase 200 kDa, 3—complex II *T. thermophilus*.

3.2. Characterization of complex II

3.2.1. Identification of subunits

According to the homology analysis, the *T. thermophilus* complex II is encoded by a single operon with the gene order *sdhCDAB*, similar to the equivalent operons in many Gram-negative bacteria. The purified enzyme consists of four polypeptides with apparent molecular masses of 64, 27, 14 and 15 kDa as indicated by SDS-PAGE analysis (Fig. 1A) which is in agreement with the theoretical molecular weights of the *sdh* operon gene products (64.0, 26.6, 13.7 and 15.4 kDa for the subunits A, B, C and D, respectively). High performance liquid chromatography with an elution gradient optimized for hydrophobic proteins was used in order to separate the subunits of purified complex II (Fig. 1B) which were subsequently analyzed by SDS-PAGE (Fig. 1C). The subunit with an apparent mass of 27 kDa elutes first with a retention time of 26 min. Both, the apparent molecular weight and the hydrophilic character of the protein indicate that this protein represents the iron–sulfur clusters-containing subunit B of the complex II. Another hydrophilic polypeptide (apparent molecular weight of 64 kDa), elutes at a retention time of 35.2 min followed by a 30-kDa protein and two small highly-hydrophobic polypeptides of 15 kDa and 14 kDa at retention times of 42.3, 49.9 and 53.3 min, respectively. The mass of 64 kDa and the more hydrophobic character compared to the subunit B, implies its identity as the subunit A, while the two small hydrophobic domains represent the subunits C and D. The 30-kDa protein that elutes between the subunits A and the two hydrophobic polypeptides was considered as an impurity since the Edman degradation showed the presence of multiple PTH amino acids. This is in agreement with the SDS-PAGE showing scattered, thin bands of protein impurities between the FAD- and the iron–sulfur cluster-containing protein subunits. Separated polypeptides, which

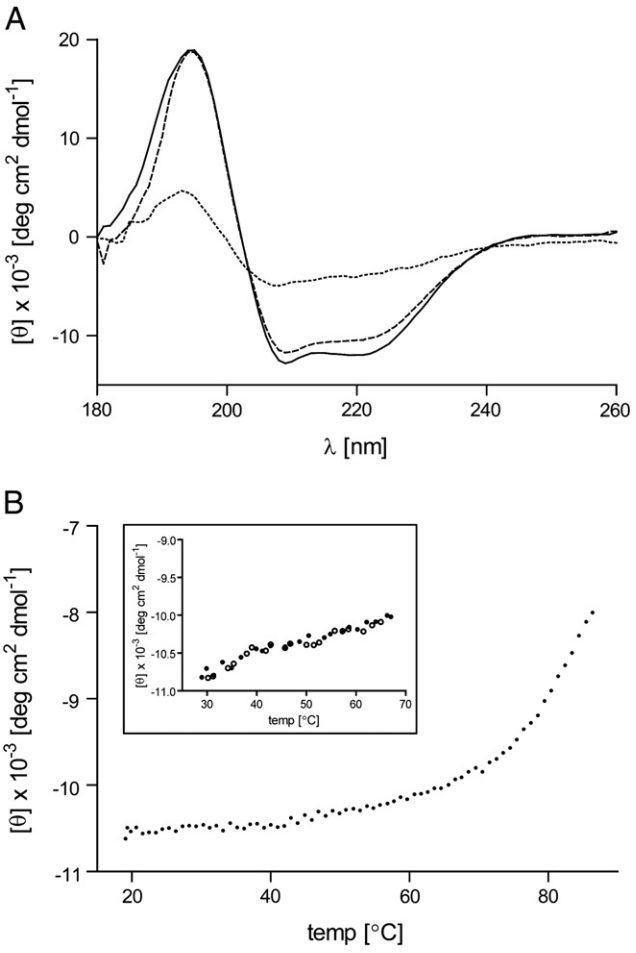

Fig. 3. Circular dichroism analysis of *T. thermophilus* complex II. A—CD spectra recorded at 20 °C (—), 70 °C (– – –) and 90 °C (···); B—the dichroic activity at 222 nm in the 20–90 °C and 30–70 °C (inset) temperature range. The data were collected with increasing (●) and subsequently decreasing (○) temperature.

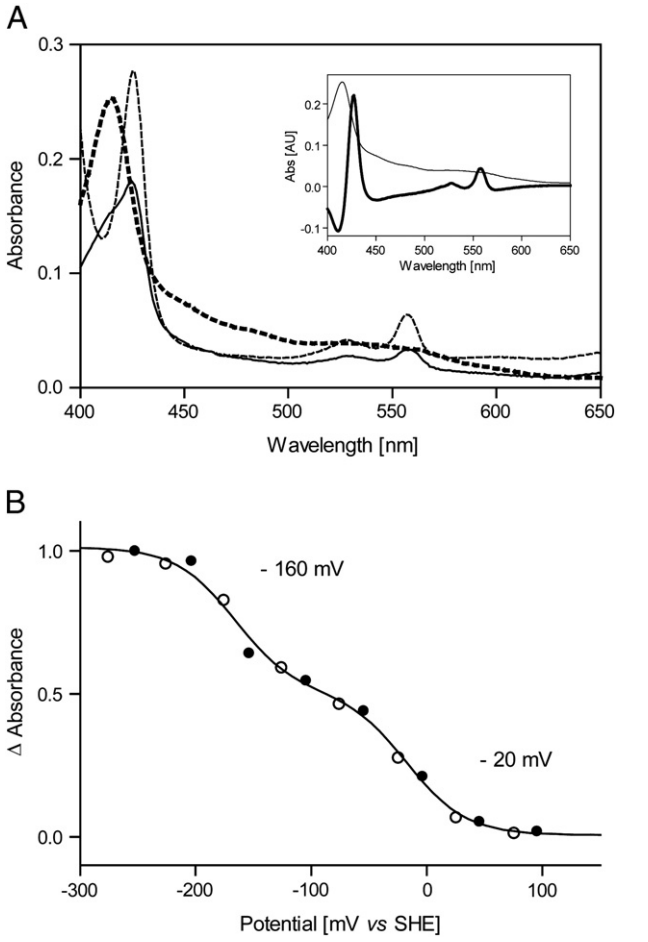

Fig. 4. Characterization of *T. thermophilus* complex II by visible spectroscopy. A—VIS spectra of complex II isolated from *T. thermophilus* in its oxidized (---), succinate-reduced (—) and dithionite-reduced (– – –) state (main) and in its oxidised (—) and fully reduced-minus-oxidised state (—) (inset); B—Optical titration of hemes b on the Soret band at 427-411 nm in oxidative (○) and reducive (●) direction, performed at room temperature and pH 7, fitted to a sum of two $n = 1$ standard Nernst equations.

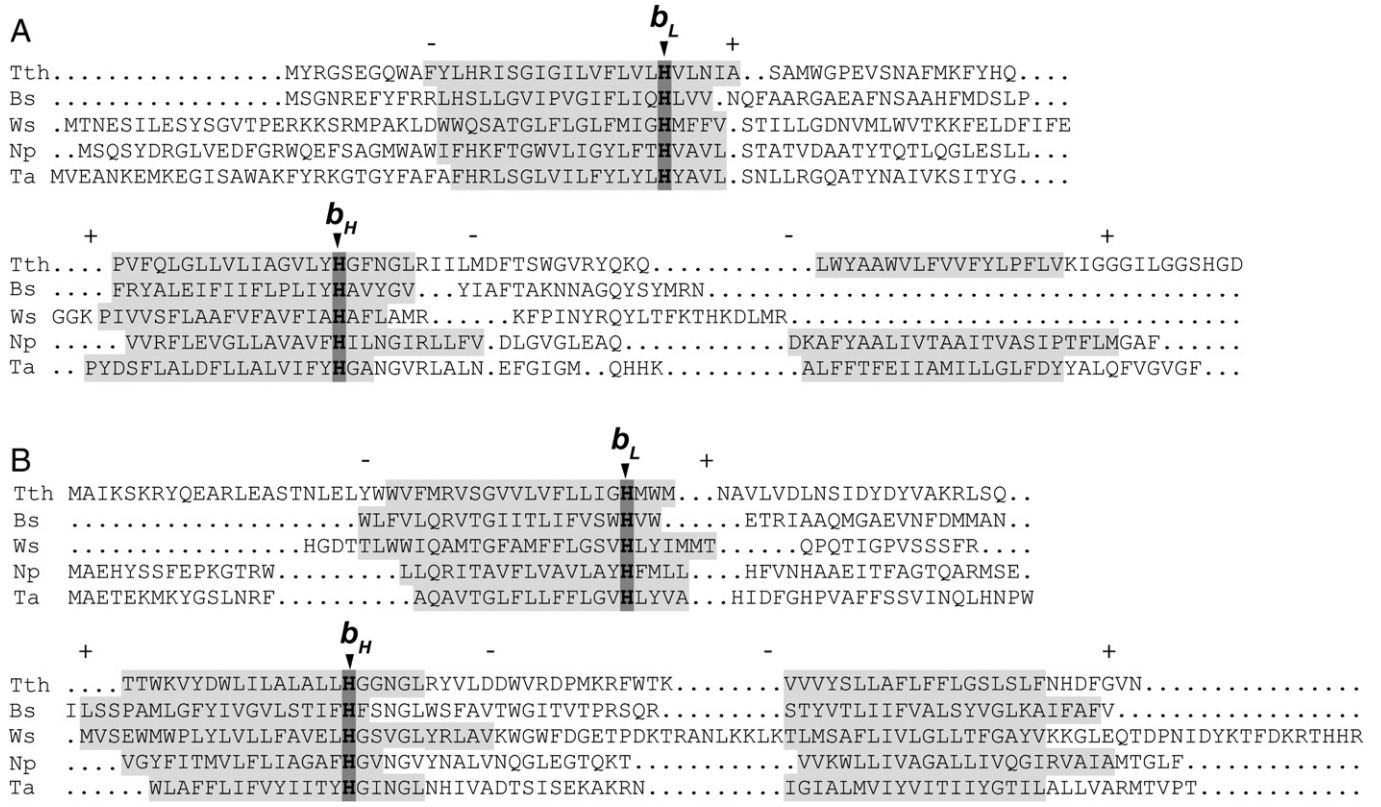

Fig. 5. Sequence comparison of SdhC (A) and SdhD (B) anchor polypeptides of di-heme SQRs. Analysed sequences of SQRs: *Bacillus subtilis* (Bs, P08064), *Wolinella succinogenes* (Ws, P17413), *Natronobacterium pharaonis* (Np, Y07709), *Thermoplasma acidophilum* (Ta, X70908) and *Thermus thermophilus* (Tth, Q5SIB8, Q5SIB9). Arrows indicate heme axial ligands. For the Type B anchors the SdhC polypeptides continue throughout A and B. Minus and plus indicate cytoplasmic and periplasmic sides, respectively. The comparison has been made by aligning the membrane spanning helices and exposed loops separately. Membrane helices were predicted with the TMPred software.

proved to have free N-termini, were subjected to Edman degradation. The sequencing results correspond to those deduced from the nucleotide sequence of the *sdh* operon from *T. thermophilus* and thus identify the gene products of *sdhDCAB* operon as genuine subunits of succinate:quinone reductase isolated from membranes of this extremophile (Table 2).

3.2.2. Oligomerisation state of the enzyme

The estimation of the molecular weight of membrane proteins is much more complicated than that based on techniques designed for soluble proteins where the results are often unambiguous. While using gel filtration chromatography as a method to evaluate the oligomerisation state of membrane proteins requires the determination of the protein:detergent:lipid ratio of the sample [33], results obtained by BN-PAGE are altered by the molecules of Coomassie Brilliant Blue G-250 (CBB) which bind to the hydrophobic patches in membrane protein exchanging the detergent molecules during electrophoresis. Due to this phenomenon, Veenhoff and co-workers proposed calculation of the apparent molecular weight of membrane proteins on BN-PAGE by multiplying their theoretical molecular weight by a factor of 1.8 [34]. A homogeneous sample of complex II, as judged by its single peak of Gaussian distribution after final size exclusion chromatography, was analyzed by BN-PAGE. The sample shows a major band that migrates slightly above one of the standard proteins—apoferritin (443 kDa; Fig. 2), and corresponds to ~500 kDa. The observed additional high molecular weight band may represent aggregates formed during the exchange of DDM by CBB during electrophoresis. Considering the calculated molecular weight of *T. thermophilus* complex II and the fact that unspecific binding of CBB originates only from the membrane subunits of the complex, the apparent molecular weight of the monomeric complex on the BN-PAGE should be ~150 kDa. The oligomerisation state which is closest to the apparent molecular weight of ~500 kDa is a trimeric form. Previous studies and several available crystal structures showed that the oligomerisation state of SQORs varies; prokaryotic QFRs are present as homodimeric complexes [20,35] while eukaryotic SQRs tend to be monomers [16,17]. The crystal structure of the *E. coli* SQR [15] and the characterization of those from *Corynebacterium glutamicum* [36] and *Bacillus licheniformis* [37] showed a homotrimeric nature of prokaryotic SQRs which is in agreement with our finding. However, the SQR from *Sulfolobus acidocaldarius* was found to be a monomer based on gel filtration studies [38].

3.2.3. Protein stability

Circular dichroism (CD), which is becoming increasingly important in structural investigations of membrane proteins [39], was used to investigate the secondary structure of the complex II and the protein thermostability. The spectrum recorded at 20 °C exhibited negative bands at ~222 and ~210 nm and a positive band at ~192 nm that are characteristic for both soluble and membrane proteins with predominantly helical structures [40]. Minor differences in the spectra can be observed after incubation of the protein at 70 °C for 15 min (Fig. 3A) suggesting limited conformational changes of the protein. Interestingly, incubation of the protein sample for the same duration at 90 °C led to severe protein precipitation (~50%) reflected by a concomitant drastic decrease of CD signal size with retainment of the overall spectral shape (Fig. 3A). The deconvolution of the spectra was consistent with protein denaturation at 90 °C as indicated by a decrease in the helical content from 48% to 21% and an increase of the disordered region from 24% to 38% in comparison to the data recorded at 20 °C. Further incubation for 30 min at 90 °C led to a complete precipitation of complex II while only ~10% of the protein precipitates during an extended incubation at 70 °C. Thermal unfolding generally occurs in a cooperative manner with clearly-defined folded and

unfolded states separated by a steep unfolding transition. From the plot relating the observed ellipticity at 222 nm to temperature (Fig. 3B) the transition to the fully unfolded state appears to require a higher temperature as a completely unfolded state of the protein is not reached. The protein denaturation temperature (T_m) therefore cannot be estimated due to the limitation of the instrument that can only operate at a maximum temperature of 90 °C. Based on the shape of the curve, however, the T_m of the *T. thermophilus* complex II can be determined to be>80 °C. It has to be noted that the loss in the CD amplitude at 222 nm, and thus thermodenaturation, is fully reversible within the temperature range up to 70 °C (Fig. 3B inset). Overall, this rather low thermostability of the *T. thermophilus* complex II compared to other enzymes isolated from this organism is unusual. The observed behavior might be caused by the delipidation of the complex during the extensive purification process the protein was subjected to.

3.2.4. Characterization of redox cofactors

Redox cofactors of the purified enzyme have been characterized using UV-Vis and EPR spectroscopy. The presence of heme *b* and the absence of other heme types in the enzyme was indicated by the pyridine ferrochrome spectrum which showed a main peak at 559 nm and a smaller peak at 528 nm [24]. The presence of a heme *b* moiety was clearly identifiable by visible redox spectroscopy. In the as-isolated form, the enzyme showed an absorption peak at 412 nm and shoulders around 450, 480, 525 and 560 nm. When reduced with succinate, absorption peaks were visible at 425 and 559 nm with a shoulder around 412 nm suggesting partial reduction of heme *b*. Subsequent addition of dithionite resulted in absorption peaks at 425, 525 and 558 nm (Fig. 4A). In the fully reduced-minus-oxidised spectrum of *T. thermophilus* complex II the absorbance for heme *b* was observed with a maximum at 427 nm for the Soret band and a single, symmetrical peak at 558 nm for the corresponding alpha band (Fig. 4A inset). The two distinct, though very close (559 and 558 nm), maxima observed after reduction with succinate and dithionite, indicate the presence of two distinct heme *b* species of slightly different spectroscopic properties.

It has been shown that the *b*-hemes in complex II contain bis-histidine axial ligation which is conserved throughout complexes II regardless of the number of heme cofactors [1,41–44]. The two heme molecules in Type A and B SQORs have been denoted as b_H and b_L (for a high and a low redox midpoint potential, respectively), while single-heme SQORs contain only b_H, although with variable midpoint potentials. Accordingly, all complexes II contain conserved histidine residues acting as the ligands to heme b_H, while in di-heme proteins additional conserved histidine residues are present—the ligands of heme b_L. The presence of the b_L ligands in *T. thermophilus* complex II is clearly visible by sequence comparison with other two-heme SQORs (Fig. 5). The existence of two heme *b* cofactors in equal amounts within *T. thermophilus* complex II has been further confirmed by optical Vis red-ox titration which revealed two titration waves (Fig. 4B). The data points were fitted to a sum of two one-electron Nernst curves with equal amplitudes and midpoint potentials of −20 mV and −160 mV relative to the standard hydrogen electrode, attributed to hemes b_H and b_L, respectively.

The existence of two heme molecules is characteristic for the SQORs from organisms using low potential quinone as electron acceptor [1,8] as electron transfer through the two heme *b* molecules

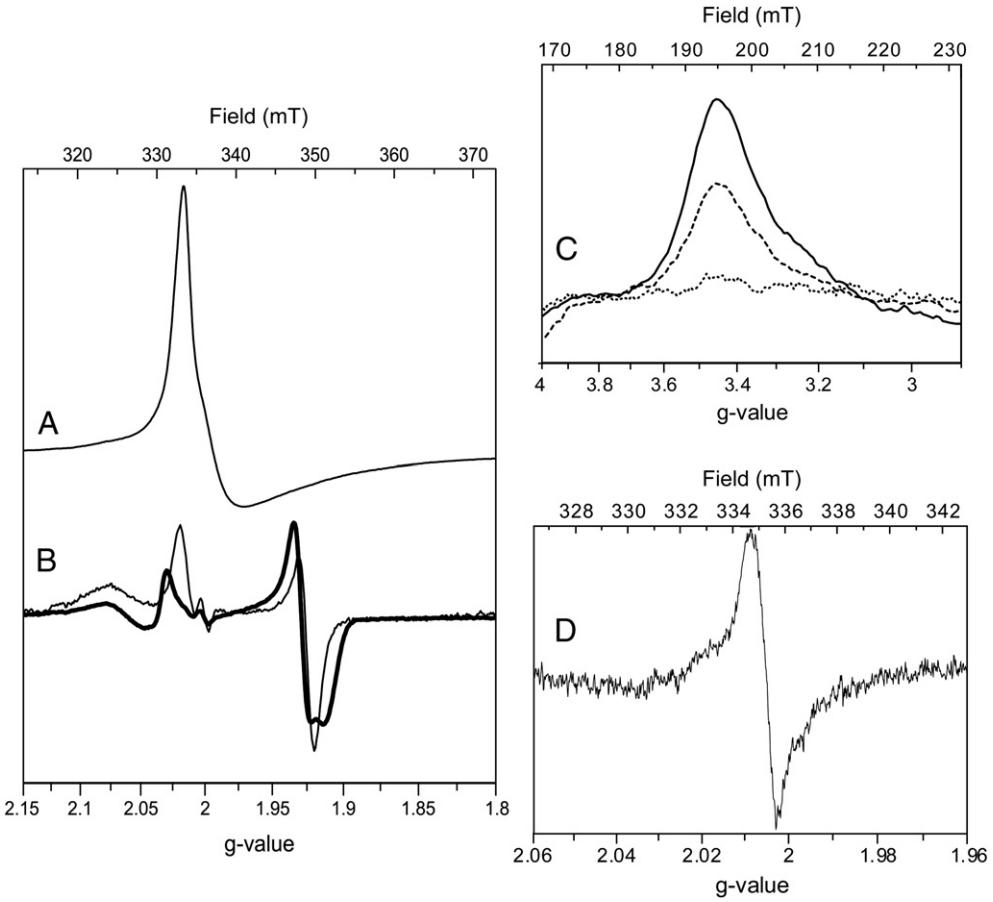

Fig. 6. EPR analysis of complex II from *T. thermophilus*. A—EPR spectrum of 70 μM complex II with no addition; B-EPR spectra of 20 μM complex II with addition of 5 mM ascorbate (–) and 120 mM succinate (—); C—EPR spectra of 70 μM complex II with no addition (−), with addition of 120 mM succinate (– – –) and dithionite (···); D—EPR spectrum of 70 μM complex II with 120 mM succinate. Spectra A, B, C and D were recorded at temperatures of 8 K, 15 K, 15 K and 100 K, microwave powers of 64 mW, 20 mW, 64 mW and 1 mW and modulation amplitudes of 1 mT, 1 mT, 3 mT and 0.2 mT, respectively. Measured microwave frequencies used to calculate the g-values were 9.41 (A–C) and 9.4105 (D).

coupled with transmembrane proton transfer is crucial to catalyze the thermodynamically unfavorable oxidation of succinate by MK *in vivo* [8,37,45,46]. This is consistent with the present results since *T. thermophilus* contains low potential menaquinones (~−80 mV) only [47,48] We therefore conclude that the purified enzyme from *T. thermophilus* belongs to the type A SQORs due to the presence of two *b*-hemes per molecule of protein and two membrane anchor polypeptides, SdhC and SdhD. To the best of our knowledge, this is the first study describing in detail a type A SQOR.

Redox titration of the type B di-heme SQR from *Bacillus subtilis* showed an influence of the inhibitor n-heptyl-4-hydroxy quinoline-N-oxide (HQNO) on the redox behavior of the *b*-hemes. It resulted either in a down-shift of the potential of heme b_L [49] or in a pronounced redox hysteresis of the entire titration curve [50] which was interpreted as redox state-dependent conformational changes in the membrane domain. We titrated complex II of *T. thermophilus* in the presence of 500 μM NQNO and observed no hysteresis and no significant influence of the inhibitor on the redox midpoint potentials of the *b*-hemes.

We further characterized the SQR from *T. thermophilus* by electron paramagnetic resonance (EPR) spectroscopy. All the cofactors expected to be present in complex II could be detected in the purified enzyme. In the oxidized form of the enzyme, EPR spectroscopy showed the presence of a [3Fe–4S] cluster with a *g* at 2.017 (Fig. 6A). This redox center was reducible by an excess of succinate. Its amplitude was strongly diminished after addition of ascorbate (Fig. 6B). We therefore estimate its redox midpoint potential to be higher than + 50 mV. In addition, a signal at $g_z = 3.45$ was present in the oxidized sample, characteristic for the presence of heme *b* (Fig. 6C). Part of the amplitude of this signal was lost upon reduction by ascorbate or succinate without modification of the position of the signal. Addition of dithionite resulted in complete loss of the signal. From the optical redox titration and the determination of heme content, we concluded that two heme cofactors are present in this enzyme, as suggested by the presence of the four conserved histidine residues in the amino acid sequence of the membrane subunits C and D. The fact that both *b*-hemes have the same EPR signature with a high g_z value indicates that the angle between the planes of their two respective histidine ligands is similar for both hemes and close to perpendicular [51]. Similar histidine arrangement was observed in the only currently available structure of a di-heme-containing SQOR, the QFR from *W. succinogenes*, where the interplanar angle is approximately 90 degrees [14,45]. In the succinate-reduced sample a radical signal at $g = 2.005$ with a peak-to-peak width of 11 G was present (Fig. 6D), characteristic of the flavin in its semiquinone state [52]. A signal of the [2Fe–2S] center appeared upon reduction by ascorbate as well as by succinate (Fig. 6B). To obtain the full amplitude of this signal, reduction by dithionite was required. Intriguingly, the rhombicity of the signal was higher in the presence of succinate than after reduction by ascorbate. In the ascorbate-reduced state the g_x trough at about 1.92 superimposed on the g_y line at 1.926, whereas in the presence of succinate the g_x trough at 1.91 was distinguishable from the g_y signal at 1.93. Further experiments are in progress to search for an explanation of this phenomenon. The saturation behavior of the g_y signal corresponding to the [2Fe–2S] cluster was similar, irrespective of the presence or absence of succinate (Fig. 7 inset), while the redox midpoint potential of this cofactor was determined by EPR titration to be −10 mV (Fig. 8).

In 1997 Hägerhäll et al. [1] reported that the respective redox midpoint potentials of the [2Fe–2S] and the [3Fe–4S] centers are a signature of the function of the enzyme. They observed that in menaquinone reducing SQRs the redox midpoint potential of the [2Fe–2S] center was above that of the [3Fe–4S] center, whereas in ubiquinone reducing SQRs the opposite situation occurs. In addition, based on the seven species available at that time, the midpoint

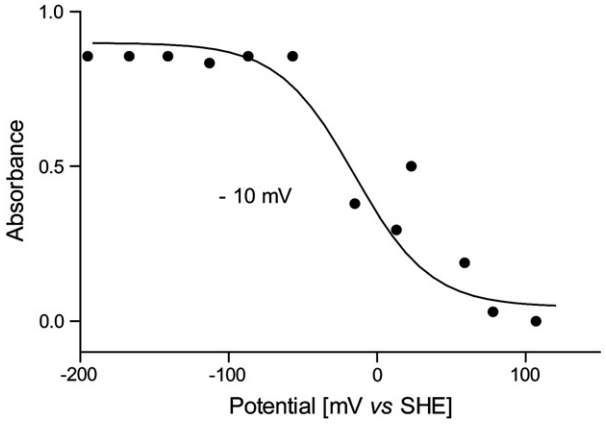

Fig. 8. EPR-based determination of the redox midpoint potential of the [2Fe–2S] cluster of *T. thermophilus* complex II. The EPR redox titration of the amplitude of the $g_y = 1.93$ signal of the [2Fe–2S] center has been fitted to an $n = 1$ standard Nernest equation with a redox midpoint potential of −10 mV.

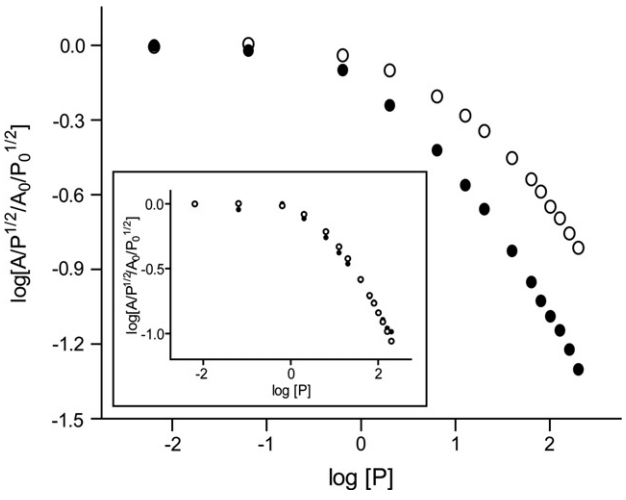

Fig. 7. EPR saturation curves of the g_y-signal of the [2Fe–2S] center of *T. thermophilus* complex II reduced with ascorbate (●) and dithionite (○) at pH 9 (main) and reduced with ascorbate (●) and succinate (○) at pH 7 (inset). Spectra were recorded at the temperature of 15 K, modulation amplitude 1 mT and microwave frequency of 9.41.

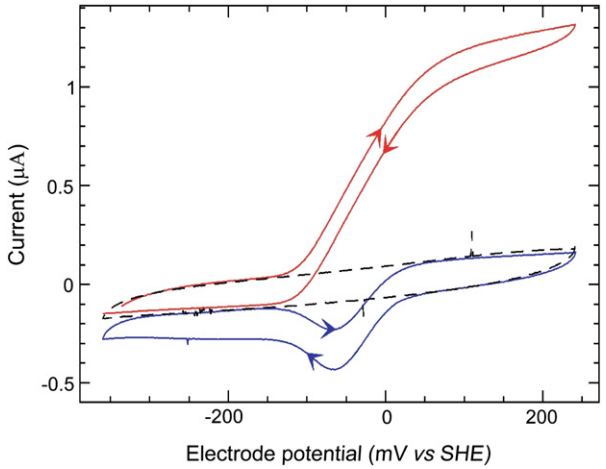

Fig. 9. Catalytic signature of *T. thermophilus* complex II in protein film voltammetry. Oxidation of 1 mM succinate at pH 8.5 (red) and reduction of 0.4 mM fumarate at pH 7 (blue) was performed at 50 °C with a scan rate of 5 mV/s and an electrode rotation rate of 3 krpm. The black dashed line is a blank recorded with no adsorbed enzyme. Arrows indicate the direction of the sweeps.

potential of the [2Fe–2S] cluster was relatively high (above + 50 mV) in menaquinone reducing SQRs, around 0 mV in ubiquinone reducing SQRs and below −20 mV in QFRs. The *T. thermophilus* enzyme with midpoint potentials of > + 50 mV and −10 mV for [3Fe–4S] and [2Fe–2S] clusters, respectively, does not conform to this classification and the potential difference between the [2Fe–2S] and the [3Fe–3S] cluster seems therefore not be a prerequisite for the uphill reduction of MK by succinate.

The presence of the [4Fe–4S] center cannot be accessed directly *via* its EPR signal, since this centre is coupled to the [2Fe–2S] cluster [53]. However, upon reduction of the [4Fe–4S] centre, the saturation behavior of the g_y signal of the [2Fe–2S] center changes, since the relaxation of this centre is enhanced by the presence of a spin on the [4Fe–4S] centre. The reduction of the [4Fe–4S] centre by dithionite could not be achieved at pH 7, indicating that the redox midpoint potential of this cofactor is lower than −300 mV (compared to −310 mV in *E. coli* QFR [54] and −210 mV in *E. coli* SQR [55]). Therefore, saturation curves were determined on the ascorbate-reduced and the dithionite-reduced sample at pH 9, *i.e.* at a pH that allows poising the sample by dithionite to −480 mV. The respective saturation curves are shown in Fig. 7 and an enhanced relaxation was indeed observed in the completely reduced sample revealing the presence of the reduced [4Fe–4S] centre.

3.2.5. Analysis of enzyme activity

Fig. 9 shows voltammograms recorded with the enzyme adsorbed to a rotating graphite electrode, which substitutes for the redox partner as it is able to donate or accept electrons [29,54]. If the electrode potential is sufficiently high, and in the presence of succinate, the electrons resulting from succinate oxidation are directly transferred from the enzyme to the electrode. This is measured as a positive current that is proportional to the product of turnover rate of the enzyme multiplied by electroactive coverage. Under reducing conditions and in the presence of fumarate, a negative current proportional to the reduction rate of fumarate is measured. The electrode is rotated at a high rate to accelerate substrate transport towards the electrode. The catalytic contribution to the signals is independent on the scan direction (the activity is in a steady-state), but electrode charging contributes to the current and adds a minor offset, the sign of which depends on the direction of the scan.

As shown in Fig. 9, the current resulting from succinate oxidation increases from zero at low potential to a certain limit at high potential as observed before for succinate oxidation by *E. coli* SQR [56] or QFR [54]. In contrast, the rate of fumarate reduction is much less pronounced under the most reducing conditions. It increases initially as the potential is taken down (the current becomes more negative) and subsequently decreases approximating to a plateau. This shape of the fumarate reduction signal discriminates SQRs from QFRs. A similar signal to the one observed for *T. thermophilus* complex II has been previously reported for soluble subunits of *E. coli* and beef heart SQRs [56–58], whereas the three fumarate reductases characterized to date using protein film voltammetry (membrane extrinsic domain (FrdAB) of QFR from *E. coli*, and soluble Fcc_3 and Ifc_3 from *Shewanella frigidimarina*) do not exhibit such a decrease in activity at low electrode potential [29]. While the cyclic voltammetry analysis of the purified, three-subunit SQR from *Bacillus subtilis* has also been performed [50], it cannot be considered for the purpose of this discussion as the fumarate reduction signal was not reported therein. Many redox enzymes exhibit complex changes in activity against driving force [29,59]. Regarding the SQRs, the molecular reasons underlying these catalytic properties have not been entirely clarified. Nevertheless the presented electrochemical signature of *T. thermophilus* complex II is clearly similar to those reported before for SQRs which supports the affiliation of *T. thermophilus* complex II as one. Furthermore, the facts that the enzyme has been purified from cells grown under aerobic conditions and that the operon encoding for it is the only SQOR-encoding operon present in the genome of this aerobic bacterium also strongly suggest that the purified enzyme is a SQR.

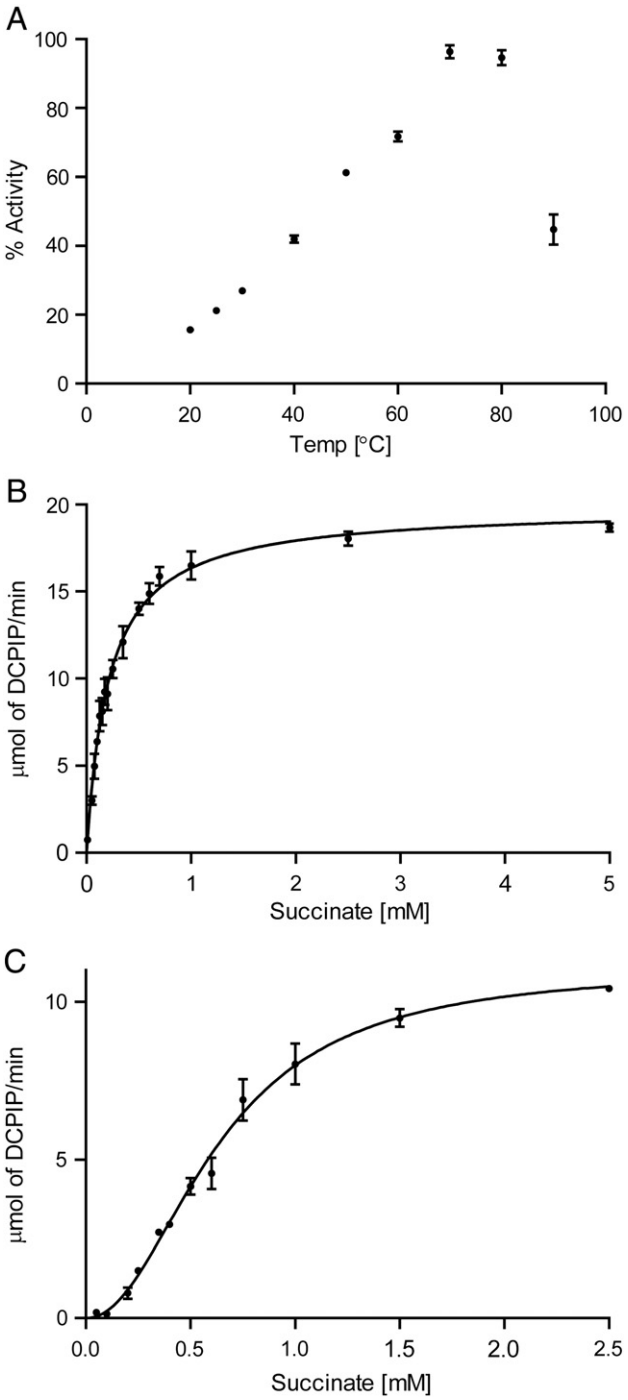

Fig. 10. Kinetic analysis of *T. thermophilus* complex II. A—Temperature profile of Thermus SQR activity. B—Michaelis–Menten kinetics of 40 nM Thermus complex II at 30 °C. C—Non-Michaelis–Menten kinetics of 10 nM Thermus complex II at 70 °C.

The succinate dehydrogenase activity of the purified enzyme has been measured using solution assays with PMS as the intermediate and DCPIP as the final electron acceptor. This, together with the findings presented above, confirms that the described procedures of protein extraction and purification resulted in the isolation of an intact, four-subunit, active enzyme. The influence of three buffers on enzyme activity has been investigated. Interestingly, the activity when measured at pH 8 in phosphate and Hepes buffers was 10 and 1.3 time lower than in Tris–HCl buffer. A significant difference in

Table 3
Comparison of K_M values for succinate oxidation of various succinate:quinone oxidoreductases.

Organism	Enzyme	K_M (mM)	Reference
Thermus thermophilus[a]	SQR	0.21 (30 °C)	this work
Rhodothermus marinus[a]	SQR	0.165 (65 °C)	[62]
Sulfolobus acidocaldarius[a]	SQR	1.42 (55 °C)	[38]
Thermoplasma acidophilum[a]	membranes	0.32 (53 °C)	[63]
Corynebacterium glutamicum	SQR	0.25	[36]
Bacillus sp. strain YN-2000	SQR	1.42	[64]
Bacillus firmus OF4	SQR	0.30	[65]
Escherichia coli	SQR	0.071	[66]
	SQR	0.1	[67]
Bos taurus	SQR	0.02	[68]
Acidianus ambivalens	membranes	0.50	[69]
Sulfolobus strain 7	membranes	0.28	[70]
Halobacterium halobium	membranes	0.70	[71]
Plasmodium yoelii yoelii	mitochondria	0.049	[72]
Rattus Sprague–Dawley	mitochondria	0.26	[73]
Escherichia coli	QFR	1.0	[74]
	QFR	0.55	[67]
	QFR[b]	~0.1[b]	[54]
Wolinella succinogenes	QFR	7	[75]
Desulfovibrio gigas	QFR	2	[76]
Shewanella frigidimarina	QFR[c]	0.6–2.6[c]	[77]

[a] Optimal activity temperature of enzymes from *T. thermophilus*, *Rhodothermus marinus*, *Sulfolobus acidocaldarius* and *Thermoplasma acidophilum* are 70 °C, 80 °C, 81 °C and 78 °C, respectively, while K_M for those were established at temperatures given in brackets.
[b] The experiments have been performed for soluble part of the QFR (FrdAB) and established K_M was 0.083 mM and 0.13 mM in pH of 7.5 and 8, respectively.
[c] Fumarate reductase from Shewanella frigidimarina is, unlike other enzymes listed herein, is a soluble protein. Reported K_M values were determined in the pH range from 8 to 10.

enzyme activity was observed between pH 7 and 8 in all analyzed buffers (two to three times higher activity at pH 8) while the difference observed with the increase of pH above 8.5 was negligible. Activity reached the optimum at 70 °C, which is the optimal growth temperature of *T. thermophilus* (Fig. 10A). The sudden decrease of enzyme activity above 70 °C is caused by the instability of the enzyme at a higher temperature (see 3.2.3). The enzyme displays the standard Michaelis–Menten kinetics at 30 °C with a K_M of 0.21 mM and a k_{cat} of 500 min^{-1} (Fig. 10B); all the SQORs described previously exhibit Michaelis–Menten kinetics and their K_M values for succinate are summarized in Table 3. Compared with the K_M of the other SQRs, the K_M of the *T. thermophilus* enzyme is relatively low, demonstrating its high affinity for the substrate. Interestingly, however, at 70 °C the plot of initial velocity *vs.* succinate concentration shows a deviation from the standard Michaelis–Menten kinetics. This is reflected in the sigmoidal shape of the curve which is a classic signature for cooperatively interacting active sites. Considering the high purity of this oligomeric enzyme and the fact that this phenomenon is observed specifically at higher temperatures, it can be assumed that the deviation from Michaelis–Menten kinetics is a result of cooperativity. The transition from the standard Michaelis–Menten kinetics to positive cooperativity is observed between 55 °C and 60 °C and is most likely related to the conformational changes observed for the enzyme at higher temperatures (see 3.2.3.). The experimental data fitted to a positive cooperative model resulted in a k' of 0.39 mM and a Hill coefficient h of 2.105 at 70 °C. This suggests a moderate positive cooperativity and at least three binding sites on the oligomeric enzyme. Considering the trimeric nature of the enzyme it is possible that the minimum number of binding sites determined by h is the actual number of substrate binding sites with one site per protomer. However, the mechanism by which a protomer may sense binding of succinate on a neighboring subunit remains to be determined. The temperature-induced cooperativity is a known phenomenon and it has recently been observed in the alcohol dehydrogenase from the thermoacidophilic crenarchaeon *Solfolobus solfataricus* [60] and this is, to our knowledge, the first report of cooperativity in succinate:quinone oxidoreductase. As mentioned before, all the SQORs characterized to date exhibit Michaelis–Menten kinetics (Table 3). However, the K_M for three SQRs from thermophilic species (*Rhodothermus marinus, Thermoplasma acidophilum* and *Solfolobus acidocaldarius*) were analyzed at temperatures significantly lower than the enzyme optimum, most likely due to technical difficulties at high temperatures. Although in the first two cases these were optimal or close to optimal growth temperatures of the parent organisms, it cannot be excluded that these enzymes also may exhibit different characteristics when analyzed at their optimal temperatures, especially for *S. acidocaldarius*.

The influence of standard inhibitors on the succinate dehydrogenase activity of the *T. thermophilus* SQR has been tested using the PMS/DCPIP assay at 30 °C. Sodium malonate and sodium diethyl oxalacetate inhibited the complex II in a competitive fashion with inhibition constants (K_i) of 40 μM and 17 μM, respectively, while K_i for a suicide inhibitor 3-nitropropionic acid has been determined as 0.23 mM (data not shown). NQNO, a semiquinone analog had a negligible effect on the succinate dehydrogenase activity assayed with PMS/DCPIP as expected based on previous reports [1,36,61]. The activity was also measured with or without various quinone analogs as the direct electron acceptors (Table 4). With DCPIP as the only electron acceptor, the activity decreased five fold in comparison to assays in the presence of PMS. Addition of 1,4-naphthoquinone (1,4-NQ) increased the DCPIP activity by a factor of two. The DCPIP/1,4-NQ activity was inhibited by NQNO in non-competitive manner with a K_i of 70 μM, indicating a relatively low sensitivity of the enzyme to this inhibitor. Activity measurements with duroquinone (DQ)/DCPIP or with Vitamine K_3 (Vit. K_3)/DCPIP gave values close to those observed with DCPIP only (Table 4). In the presence of p-benzoquinone (p-BQ)

Table 4
Comparison of succinate dehydrogenase activity of *T. thermophilus* SQR with various quinones, PMS and DCPIP.

Quinone	Succinate dehydrogenase activity k_{cat} (min^{-1})
PMS/DCPIP	500
DCPIP	110
menadione (Vit. K_3)/DCPIP	100
duroquinone/DCPIP	130
1,4-naphthoquinone/DCPIP	220
p-benzoquinone/DCPIP	0

Fig. 11. Crystals of *T. thermophilus* complex II obtained in 0.1 M magnesium chloride, 0.1 M sodium acetate pH 4.6 and 12% PEG 6000 as precipitant.

no activity could be measured with DCPIP. Addition of p-BQ to the PMS/DCPIP assay lowered the activity by factor of 1.5.

The increase of measured activity with 1,4-NQ/DCPIP with respect to DCPIP showed that the membrane part of the enzyme, that harbors the quinone binding sites, is functional in the purified state. Vit. K_3 and DQ did not show any effect on enzyme activity, most probably because these hydrophilic molecules have no access to the quinone binding sites. Decreased turnover numbers in the DCPIP and in the PMS/DCPIP assay in the presence of p-BQ were observed previously for the *C. glutamicum* SQRs [36]. This behavior has been interpreted as an inhibition effect of the quinone. We would like to consider another explanation. p-BQ has a redox midpoint potential of + 280 mV whereas DCPIP is at + 217 mV and PMS at + 80 mV. Electron transfer from p-BQ to DCPIP is therefore not favorable, especially if the transfer of the first electron from p-BQ occurs at even higher potential due to the redox chemistry of quinones. p-BQ may therefore be a good electron acceptor of complex II but a very poor donor to DCPIP. This interpretation is in line with the observation that p-BQ lowers the turnover numbers measured in the presence of PMS and DCPIP. PMS is a small mediator, supposed to be able to accept electrons directly from the iron sulfur clusters, especially the [3Fe–4S] cluster. It should therefore be able to get reduced by complex II, even if its quinone binding site(s) is/are blocked, as it is the case in the presence of NQNO that fails to affect the turnover in the presence of PMS. If p-BQ, however, is an electron acceptor of complex II electron transfer to PMS and to p-BQ will be in competition. Consequently DCPIP reduction *via* PMS will be lower in the presence of p-BQ. Unfortunately, direct measurements of quinone reduction by complex II is impeded by the strong absorbance of fumarate in the UV region.

3.3. Crystallization and concluding remarks

The characterization of the succinate:quinone reductase from *T. thermophilus* revealed some interesting features which were not observed with other SQORs. Further studies on this subject are in progress. Sitting drop vapour diffusion crystallisation trials of the *T. thermophilus* complex II have been initiated; the conditions resulting in initial hits were subjected to a series of extensive optimizations and gave optically perfect crystals of dimensions up to $160 \times 50 \times 40$ μm (Fig. 11). However, these crystals diffracted only up to 7 Å; further optimisation is therefore required. While doing so, we extended our studies to the production of recombinant enzyme. The higher production levels of the protein, a simpler purification procedure and the feasibility of site-directed mutagenesis studies should significantly facilitate our research on this interesting enzyme.

Acknowledgments

This work was supported by the Science Fundation Ireland BICF685 and SFI Ulysses Research Visit to France 2009 to TS and by the French National Centre for Scientific Research (CNRS).

References

[1] C. Hägerhäll, Succinate: quinone oxidoreductases. Variations on a conserved theme, Biochim Biophys Acta 1320 (1997) 107–141.
[2] M. Saraste, Oxidative phosphorylation at the fin de siecle, Science 283 (1999) 1488–1493.
[3] A. Kröger, V. Geisler, E. Lemma, F. Theis, R. Lenger, Bacterial fumarate respiration, Arch Microbiol 158 (1992) 311–314.
[4] J.R. Guest, Partial replacement of succinate dehydrogenase function by phage- and plasmid-specified fumarate reductase in *Escherichia coli*, J Gen Microbiol 122 (1981) 171–179.
[5] E. Maklashina, D.A. Berthold, G. Cecchini, Anaerobic expression of *Escherichia coli* succinate dehydrogenase: functional replacement of fumarate reductase in the respiratory chain during anaerobic growth, J Bacteriol 180 (1998) 5989–5996.
[6] C.R. Lancaster, Succinate:quinone oxidoreductases: an overview, Biochim Biophys Acta 1553 (2002) 1–6.
[7] T. Ohnishi, C.C. Moser, C.C. Page, P.L. Dutton, T. Yano, Simple redox-linked proton-transfer design: new insights from structures of quinol-fumarate reductase, Structure 8 (2000) R23–R32.
[8] J. Schirawski, G. Unden, Menaquinone-dependent succinate dehydrogenase of bacteria catalyzes reversed electron transport driven by the proton potential, Eur J Biochem 257 (1998) 210–215.
[9] L. Hederstedt, Respiration without O_2, Science 284 (1999) 1941–1942.
[10] C.R. Lancaster, A. Kroger, Succinate: quinone oxidoreductases: new insights from X-ray crystal structures, Biochim Biophys Acta 1459 (2000) 422–431.
[11] R.S. Lemos, A.S. Fernandes, M.M. Pereira, C.M. Gomes, M. Teixeira, Quinol: fumarate oxidoreductases and succinate:quinone oxidoreductases: phylogenetic relationships, metal centres and membrane attachment, Biochim Biophys Acta 1553 (2002) 158–170.
[12] H.D. Juhnke, H. Hiltscher, H.R. Nasiri, H. Schwalbe, C.R. Lancaster, Production, characterization and determination of the real catalytic properties of the putative 'succinate dehydrogenase' from *Wolinella succinogenes*, Mol Microbiol 71 (2009) 1088–1101.
[13] T.M. Iverson, C. Luna-Chavez, G. Cecchini, D.C. Rees, Structure of the *Escherichia coli* fumarate reductase respiratory complex, Science 284 (1999) 1961–1966.
[14] C.R. Lancaster, A. Kroger, M. Auer, H. Michel, Structure of fumarate reductase from *Wolinella succinogenes* at 2.2 Å resolution, Nature 402 (1999) 377–385.
[15] V. Yankovskaya, R. Horsefield, S. Tornroth, C. Luna-Chavez, H. Miyoshi, C. Leger, B. Byrne, G. Cecchini, S. Iwata, Architecture of succinate dehydrogenase and reactive oxygen species generation, Science 299 (2003) 700–704.
[16] L.S. Huang, G. Sun, D. Cobessi, A.C. Wang, J.T. Shen, E.Y. Tung, V.E. Anderson, E.A. Berry, 3-nitropropionic acid is a suicide inhibitor of mitochondrial respiration that, upon oxidation by complex II, forms a covalent adduct with a catalytic base arginine in the active site of the enzyme, J Biol Chem 281 (2006) 5965–5972.
[17] F. Sun, X. Huo, Y. Zhai, A. Wang, J. Xu, D. Su, M. Bartlam, Z. Rao, Crystal structure of mitochondrial respiratory membrane protein complex II, Cell 121 (2005) 1043–1057.
[18] K. Nakamura, M. Yamaki, M. Sarada, S. Nakayama, C.R. Vibat, R.B. Gennis, T. Nakayashiki, H. Inokuchi, S. Kojima, K. Kita, Two hydrophobic subunits are essential for the heme *b* ligation and functional assembly of complex II (succinate-ubiquinone oxidoreductase) from *Escherichia coli*, J Biol Chem 271 (1996) 521–527.
[19] Q.M. Tran, R.A. Rothery, E. Maklashina, G. Cecchini, J.H. Weiner, *Escherichia coli* succinate dehydrogenase variant lacking the heme *b*, Proc Natl Acad Sci USA 104 (2007) 18007–18012.
[20] Y. Xin, Y.K. Lu, R. Fromme, P. Fromme, R.E. Blankenship, Purification, characterization and crystallization of menaquinol:fumarate oxidoreductase from the green filamentous photosynthetic bacterium *Chloroflexus aurantiacus*, Biochim Biophys Acta 1787 (2009) 86–96.
[21] R.G. Efremov, R. Baradaran, L.A. Sazanov, The architecture of respiratory complex I, Nature 465 (2010) 441–445.
[22] T. Soulimane, G. Buse, G.P. Bourenkov, H.D. Bartunik, R. Huber, M.E. Than, Structure and mechanism of the aberrant ba_3-cytochrome *c* oxidase from *Thermus thermophilus*, EMBO J 19 (2000) 1766–1776.
[23] T. Soulimane, R. Kiefersauer, M.E. Than, ba_3-cytochrome *c* oxidase from *Thermus thermophilus*: purification, crystallisation and crystal transformation, A Practical Guide to Membrane Protein Purification and Crystallization, Academic Press, 2002, pp. 229–251.
[24] E.A. Berry, B.L. Trumpower, Simultaneous determination of hemes a, b, and c from pyridine hemochrome spectra, Anal Biochem 161 (1987) 1–15.
[25] P. Edman, G. Begg, A protein sequenator, Eur J Biochem 1 (1967) 80–91.
[26] V. Reisinger, L.A. Eichacker, Analysis of membrane protein complexes by blue native PAGE, Proteomics 6 (Suppl. 2) (2006) 6–15.
[27] G. Bohm, R. Muhr, R. Jaenicke, Quantitative analysis of protein far UV circular dichroism spectra by neural networks, Protein Eng 5 (1992) 191–195.
[28] P.L. Dutton, Oxidation-reduction potential dependence of the interaction of cytochromes, bacteriochlorophyll and carotenoids at 77 degrees K in chromatophores of *Chromatium* D and *Rhodopseudomonas gelatinosa*, Biochim Biophys Acta 226 (1971) 63–80.
[29] C. Léger, P. Bertrand, Direct electrochemistry of redox enzymes as a tool for mechanistic studies, Chem Rev 108 (2008) 2379–2438.
[30] P.P. Liebgott, F. Leroux, B. Burlat, S. Dementin, C. Baffert, T. Lautier, V. Fourmond, P. Ceccaldi, C. Cavazza, I. Meynial-Salles, P. Soucaille, J.C. Fontecilla-Camps, B. Guigliarelli, P. Bertrand, M. Rousset, C. Léger, Relating diffusion along the substrate tunnel and oxygen sensitivity in hydrogenase, Nat Chem Biol 6 (2010) 63–70.
[31] C. Hägerhäll, R. Aasa, C. von Wachenfeldt, L. Hederstedt, Two hemes in *Bacillus subtilis* succinate:menaquinone oxidoreductase (complex II), Biochemistry 31 (1992) 7411–7421.
[32] T. Soulimane, S.R. O'Kane, O. Kolaj, Isolation and purification of *Thermus thermophilus* HpaB by a crystallization approach, Acta Crystallogr. Sect. F Struct. Biol. Cryst. Commun. 66 352-6.
[33] Y. Wei, H. Li, D. Fu, Oligomeric state of the *Escherichia coli* metal transporter YiiP, J Biol Chem 279 (2004) 39251–39259.
[34] E.H. Heuberger, L.M. Veenhoff, R.H. Duurkens, R.H. Friesen, B. Poolman, Oligomeric state of membrane transport proteins analyzed with blue native electrophoresis and analytical ultracentrifugation, J Mol Biol 317 (2002) 591–600.
[35] M. Mileni, F. MacMillan, C. Tziatzios, K. Zwicker, A.H. Haas, W. Mantele, J. Simon, C.R. Lancaster, Heterologous production in *Wolinella succinogenes* and characterization of the quinol:fumarate reductase enzymes from *Helicobacter pylori* and *Campylobacter jejuni*, Biochem J 395 (2006) 191–201.

[36] T. Kurokawa, J. Sakamoto, Purification and characterization of succinate: menaquinone oxidoreductase from *Corynebacterium glutamicum*, Arch Microbiol 183 (2005) 317–324.
[37] M.G. Madej, H.R. Nasiri, N.S. Hilgendorff, H. Schwalbe, G. Unden, C.R. Lancaster, Experimental evidence for proton motive force-dependent catalysis by the diheme-containing succinate:menaquinone oxidoreductase from the Gram-positive bacterium *Bacillus licheniformis*, Biochemistry 45 (2006) 15049–15055.
[38] R. Moll, G. Schafer, Purification and characterisation of an archaebacterial succinate dehydrogenase complex from the plasma membrane of the thermo-acidophile *Sulfolobus acidocaldarius*, Eur J Biochem 201 (1991) 593–600.
[39] B.A. Wallace, R.W. Janes, Synchrotron radiation circular dichroism spectroscopy of proteins: secondary structure, fold recognition and structural genomics, Curr Opin Chem Biol 5 (2001) 567–571.
[40] B.A. Wallace, J.G. Lees, A.J. Orry, A. Lobley, R.W. Janes, Analyses of circular dichroism spectra of membrane proteins, Protein Sci 12 (2003) 875–884.
[41] C. Hägerhäll, L. Hederstedt, A structural model for the membrane-integral domain of succinate: quinone oxidoreductases, FEBS Lett 389 (1996) 25–31.
[42] H. Friden, M.R. Cheesman, L. Hederstedt, K.K. Andersson, A.J. Thomson, Low temperature EPR and MCD studies on cytochrome b_{558} of the *Bacillus subtilis* succinate: quinone oxidoreductase indicate bis-histidine coordination of the heme iron, Biochim Biophys Acta 1041 (1990) 207–215.
[43] J. Peterson, C. Vibat, R.B. Gennis, Identification of the axial heme ligands of cytochrome b_{556} in succinate: ubiquinone oxidoreductase from *Escherichia coli*, FEBS Lett 355 (1994) 155–156.
[44] B.R. Crouse, C.A. Yu, L. Yu, M.K. Johnson, Spectroscopic identification of the axial ligands of cytochrome b_{560} in bovine heart succinate-ubiquinone reductase, FEBS Lett 367 (1995) 1–4.
[45] M.G. Madej, H.R. Nasiri, N.S. Hilgendorff, H. Schwalbe, C.R. Lancaster, Evidence for transmembrane proton transfer in a dihaem-containing membrane protein complex, EMBO J 25 (2006) 4963–4970.
[46] M.G. Madej, F.G. Muller, J. Ploch, C.R. Lancaster, Limited reversibility of transmembrane proton transfer assisting transmembrane electron transfer in a dihaem-containing succinate:quinone oxidoreductase, Biochim Biophys Acta 1787 (2009) 593–600.
[47] M.D. Collins, D. Jones, Distribution of isoprenoid quinone structural types in bacteria and their taxonomic implication, Microbiol Rev 45 (1981) 316–354.
[48] E.R. Redfarn, R. Powls, The quinones of green photosynthetic bacteria, Biochem J 106 (1968).
[49] I.A. Smirnova, C. Hagerhall, A.A. Konstantinov, L. Hederstedt, HOQNO interaction with cytochrome *b* in succinate:menaquinone oxidoreductase from *Bacillus subtilis*, FEBS Lett 359 (1995) 23–26.
[50] A. Christenson, T. Gustavsson, L. Gorton, C. Hagerhall, Direct and mediated electron transfer between intact succinate:quinone oxidoreductase from *Bacillus subtilis* and a surface modified gold electrode reveals redox state-dependent conformational changes, Biochim Biophys Acta 1777 (2008) 1203–1210.
[51] T. Teschner, L. Yatsunyk, V. Schunemann, H. Paulsen, H. Winkler, C. Hu, W.R. Scheidt, F.A. Walker, A.X. Trautwein, Models of the membrane-bound cytochromes: Mössbauer spectra of crystalline low-spin ferriheme complexes having axial ligand plane dihedral angles ranging from 0 degree to 90 degrees, J Am Chem Soc 128 (2006) 1379–1389.
[52] T. Ohnishi, T.E. King, J.C. Salerno, H. Blum, J.R. Bowyer, T. Maida, Thermodynamic and electron paramagnetic resonance characterization of flavin in succinate dehydrogenase, J Biol Chem 256 (1981) 5577–5582.
[53] H. Beinert, B.A. Ackrell, A.D. Vinogradov, E.B. Kearney, T.P. Singer, Interrelations of reconstitution activity, reactions with electron acceptors, and iron–sulfur centers in succinate dehydrogenase, Arch Biochem Biophys 182 (1977) 95–106.
[54] C. Léger, K. Heffron, H.R. Pershad, E. Maklashina, C. Luna-Chavez, G. Cecchini, B.A. Ackrell, F.A. Armstrong, Enzyme electrokinetics: energetics of succinate oxidation by fumarate reductase and succinate dehydrogenase, Biochemistry 40 (2001) 11234–11245.
[55] V.W. Cheng, E. Ma, Z. Zhao, R.A. Rothery, J.H. Weiner, The iron–sulfur clusters in *Escherichia coli* succinate dehydrogenase direct electron flow, J Biol Chem 281 (2006) 27662–27668.
[56] A. Sucheta, B.A. Ackrell, B. Cochran, F.A. Armstrong, Diode-like behaviour of a mitochondrial electron-transport enzyme, Nature 356 (1992) 361–362.
[57] H.R. Pershad, J. Hirst, B. Cochran, B.A. Ackrell, F.A. Armstrong, Voltammetric studies of bidirectional catalytic electron transport in *Escherichia coli* succinate dehydrogenase: comparison with the enzyme from beef heart mitochondria, Biochim Biophys Acta 1412 (1999) 262–272.
[58] J. Hirst, A. Sucheta, B.A.C. Ackrell, F.A. Armstrong, Electrocatalytic voltammetry of succinate dehydrogenase: direct quantification of the catalytic properties of a complex electron-transport enzyme, J Am Chem Soc 118 (1996) 5031–5038.
[59] V. Fourmond, B. Burlat, S. Dementin, M. Sabaty, P. Arnoux, E. Etienne, B. Guigliarelli, P. Bertrand, D. Pignol, C. Léger, Dependence of catalytic activity on driving force in solution assays and protein film voltammetry: insights from the comparison of nitrate reductase mutants, Biochemistry 49 (2010) 2424–2432.
[60] A. Giordano, F. Febbraio, C. Russo, M. Rossi, C.A. Raia, Evidence for co-operativity in coenzyme binding to tetrameric *Sulfolobus solfataricus* alcohol dehydrogenase and its structural basis: fluorescence, kinetic and structural studies of the wild-type enzyme and non-co-operative N249Y mutant, Biochem J 388 (2005) 657–667.
[61] C. Hagerhall, H. Friden, R. Aasa, L. Hederstedt, Transmembrane topology and axial ligands to hemes in the cytochrome *b* subunit of *Bacillus subtilis* succinate: menaquinone reductase, Biochemistry 34 (1995) 11080–11089.
[62] A.S. Fernandes, M.M. Pereira, M. Teixeira, The succinate dehydrogenase from the thermohalophilic bacterium *Rhodothermus marinus*: redox-Bohr effect on heme b_L, J Bioenerg Biomembr 33 (2001) 343–352.
[63] S. Anemuller, T. Hettmann, R. Moll, M. Teixeira, G. Schafer, EPR characterization of an archaeal succinate dehydrogenase in the membrane-bound state, Eur J Biochem 232 (1995) 563–568.
[64] M.H. Qureshi, T. Fujiwara, Y. Fukumori, Succinate:quinone oxidoreductase (complex II) containing a single heme *b* in facultative alkaliphilic *Bacillus sp.* strain YN-2000, J Bacteriol 178 (1996) 3031–3036.
[65] R. Gilmour, T.A. Krulwich, Purification and characterization of the succinate dehydrogenase complex and CO-reactive *b*-type cytochromes from the facultative alkaliphile *Bacillus firmus* OF4, Biochim Biophys Acta 1276 (1996) 57–63.
[66] K. Kita, C.R. Vibat, S. Meinhardt, J.R. Guest, R.B. Gennis, One-step purification from *Escherichia coli* of complex II (succinate: ubiquinone oxidoreductase) associated with succinate-reducible cytochrome b_{556}, J Biol Chem 264 (1989) 2672–2677.
[67] E. Maklashina, T.M. Iverson, Y. Sher, V. Kotlyar, J. Andrell, O. Mirza, J.M. Hudson, F.A. Armstrong, R.A. Rothery, J.H. Weiner, G. Cecchini, Fumarate reductase and succinate oxidase activity of *Escherichia coli* complex II homologs are perturbed differently by mutation of the flavin binding domain, J Biol Chem 281 (2006) 11357–11365.
[68] P.R. Tushurashvili, E.V. Gavrikova, A.N. Ledenev, A.D. Vinogradov, Studies on the succinate dehydrogenating system. Isolation and properties of the mitochondrial succinate-ubiquinone reductase, Biochim Biophys Acta 809 (1985) 145–159.
[69] C.M. Gomes, R.S. Lemos, M. Teixeira, A. Kletzin, H. Huber, K.O. Stetter, G. Schafer, S. Anemuller, The unusual iron sulfur composition of the *Acidianus ambivalens* succinate dehydrogenase complex, Biochim Biophys Acta 1411 (1999) 134–141.
[70] T. Iwasaki, T. Wakagi, T. Oshima, Resolution of the aerobic respiratory system of the thermoacidophilic archaeon, *Sulfolobus sp.* strain 7. III. The archaeal novel respiratory complex II (succinate:caldariellaquinone oxidoreductase complex) inherently lacks heme group, J Biol Chem 270 (1995) 30902–30908.
[71] C.H. Gradin, L. Hederstedt, H. Baltscheffsky, Soluble succinate dehydrogenase from the halophilic archaebacterium, *Halobacterium halobium*, Arch Biochem Biophys 239 (1985) 200–205.
[72] K. Kawahara, T. Mogi, T.Q. Tanaka, M. Hata, H. Miyoshi, K. Kita, Mitochondrial dehydrogenases in the aerobic respiratory chain of the rodent malaria parasite *Plasmodium yoelii yoelii*, J Biochem 145 (2009) 229–237.
[73] P. Munujos, J. Coll-Canti, F. Gonzalez-Sastre, F.J. Gella, Assay of succinate dehydrogenase activity by a colorimetric-continuous method using iodonitrotetrazolium chloride as electron acceptor, Anal Biochem 212 (1993) 506–509.
[74] W.J. Ingledew, R.K. Poole, The respiratory chains of *Escherichia coli*, Microbiol Rev 48 (1984) 222–271.
[75] G. Unden, H. Hackenberg, A. Kroger, Isolation and functional aspects of the fumarate reductase involved in the phosphorylative electron transport of *Vibrio succinogenes*, Biochim Biophys Acta 591 (1980) 275–288.
[76] R.S. Lemos, C.M. Gomes, J. LeGall, A.V. Xavier, M. Teixeira, The quinol:fumarate oxidoreductase from the sulphate reducing bacterium *Desulfovibrio gigas*: spectroscopic and redox studies, J Bioenerg Biomembr 34 (2002) 21–30.
[77] K.L. Turner, M.K. Doherty, H.A. Heering, F.A. Armstrong, G.A. Reid, S.K. Chapman, Redox properties of flavocytochrome c_3 from *Shewanella frigidimarina* NCIMB400, Biochemistry 38 (1999) 3302–3309.